



## City Research Online

### City, University of London Institutional Repository

---

**Citation:** Dissanayake, D. M. M. P., Zhou, C., Poologanathan, K., Gunalan, S., Tsavdaridis, K. D. ORCID: 0000-0001-8349-3979 and Guss, J. (2021). Numerical simulation and design of stainless steel hollow flange beams under shear. *Journal of Constructional Steel Research*, 176, 106414. doi: 10.1016/j.jcsr.2020.106414

This is the accepted version of the paper.

This version of the publication may differ from the final published version.

---

**Permanent repository link:** <https://openaccess.city.ac.uk/id/eprint/27024/>

**Link to published version:** <http://dx.doi.org/10.1016/j.jcsr.2020.106414>

**Copyright:** City Research Online aims to make research outputs of City, University of London available to a wider audience. Copyright and Moral Rights remain with the author(s) and/or copyright holders. URLs from City Research Online may be freely distributed and linked to.

**Reuse:** Copies of full items can be used for personal research or study, educational, or not-for-profit purposes without prior permission or charge. Provided that the authors, title and full bibliographic details are credited, a hyperlink and/or URL is given for the original metadata page and the content is not changed in any way.

---

City Research Online:

<http://openaccess.city.ac.uk/>

[publications@city.ac.uk](mailto:publications@city.ac.uk)

---



## City Research Online

### City, University of London Institutional Repository

---

**Citation:** Dissanayake, DMMP, Zhou, C, Poologanathan, K, Gunalan, S, Tsavdaridis, KD ORCID: 0000-0001-8349-3979 and Guss, J (2021). Numerical simulation and design of stainless steel hollow flange beams under shear. *Journal of Constructional Steel Research*, 176, doi: 10.1016/j.jcsr.2020.106414

This is the draft version of the paper.

This version of the publication may differ from the final published version.

---

**Permanent repository link:** <https://openaccess.city.ac.uk/id/eprint/27024/>

**Link to published version:** <http://dx.doi.org/10.1016/j.jcsr.2020.106414>

**Copyright:** City Research Online aims to make research outputs of City, University of London available to a wider audience. Copyright and Moral Rights remain with the author(s) and/or copyright holders. URLs from City Research Online may be freely distributed and linked to.

**Reuse:** Copies of full items can be used for personal research or study, educational, or not-for-profit purposes without prior permission or charge. Provided that the authors, title and full bibliographic details are credited, a hyperlink and/or URL is given for the original metadata page and the content is not changed in any way.

---

City Research Online:

<http://openaccess.city.ac.uk/>

[publications@city.ac.uk](mailto:publications@city.ac.uk)

---



UNIVERSITY OF LEEDS

This is a repository copy of *Numerical Simulation and Design of Stainless Steel Hollow Flange Beams under Shear*.

White Rose Research Online URL for this paper:  
<https://eprints.whiterose.ac.uk/166539/>

Version: Accepted Version

---

**Article:**

Dissanayake, DMMP, Zhou, C, Poologanathan, K et al. (3 more authors) (2021) Numerical Simulation and Design of Stainless Steel Hollow Flange Beams under Shear. *Journal of Constructional Steel Research*, 176. 106414. ISSN 0143-974X

<https://doi.org/10.1016/j.jcsr.2020.106414>

---

© 2020, Elsevier. This manuscript version is made available under the CC-BY-NC-ND 4.0 license <http://creativecommons.org/licenses/by-nc-nd/4.0/>.

**Reuse**

This article is distributed under the terms of the Creative Commons Attribution-NonCommercial-NoDerivs (CC BY-NC-ND) licence. This licence only allows you to download this work and share it with others as long as you credit the authors, but you can't change the article in any way or use it commercially. More information and the full terms of the licence here: <https://creativecommons.org/licenses/>

**Takedown**

If you consider content in White Rose Research Online to be in breach of UK law, please notify us by emailing [eprints@whiterose.ac.uk](mailto:eprints@whiterose.ac.uk) including the URL of the record and the reason for the withdrawal request.



[eprints@whiterose.ac.uk](mailto:eprints@whiterose.ac.uk)  
<https://eprints.whiterose.ac.uk/>

1           **Numerical Simulation and Design of Stainless Steel Hollow**  
2                           **Flange Beams under Shear**

3  
4                           **D. M. M. P. Dissanayake**

5           Faculty of Engineering and Environment, University of Northumbria,  
6                           Newcastle, UK.

7                           **C. Zhou**

8           Faculty of Engineering and Environment, University of Northumbria,  
9                           Newcastle, UK.

10                          **K. Poologanathan**

11           Faculty of Engineering and Environment, University of Northumbria,  
12                          Newcastle, UK.

13                          **S. Gunalan**

14           School of Engineering and Built Environment, Griffith University,  
15                          Queensland, Australia.

16                          **K. D. Tsavdaridis**

17           School of Civil Engineering, Faculty of Engineering and Physical Sciences, University of  
18                          Leeds, UK.

19                          **J. Guss**

20           Faculty of Engineering and Environment, University of Northumbria,  
21                          Newcastle, UK.

22  
23   **Abstract**

24   Stainless steel offers a range of benefits over conventional carbon steel in structural  
25   applications. This paper presents the detailed numerical modelling of shear response of cold-  
26   formed stainless steel hollow flange sections using finite element software package, Abaqus.  
27   The effect of geometric parameters such as section height and section thickness, and the  
28   influence of different steel grades were investigated following the validation of finite element  
29   models. From numerical results, the formation of diagonal tension fields can be clearly  
30   observed in the webs of rectangular hollow flange sections while more even distribution of the  
31   stresses in the webs is seen in triangular hollow flange sections. Further, a plastic hinge type  
32   mechanism is formed in triangular flanges at the post-failure region. The evaluation of

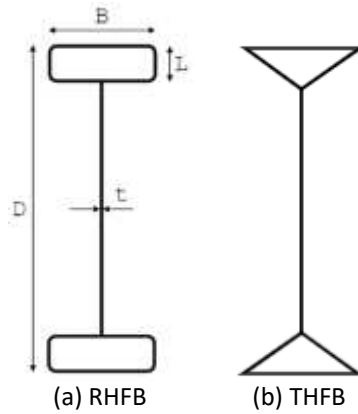
33 Eurocode 3 and the direct strength method shear design provisions for stainless steel hollow  
34 flange beams are found to be significantly conservative. Therefore, modified provisions were  
35 proposed and the comparison of those with finite element results confirmed the accurate and  
36 consistent shear resistance predictions over the codified provisions.

37 *Keywords: Cold-formed stainless steel, Hollow flange sections, Finite element modelling,*  
38 *Shear, Eurocode 3, Direct strength method*

## 39 **1 Introduction**

40 The increasing demand for stainless steel as a construction material can be seen over the other  
41 materials in the past few decades [1]. The key feature of stainless steel is its corrosion resistance  
42 making stainless steel structural components more durable while being recyclable material  
43 points out stainless steel as a sustainable solution to construction wastes. Even though, stainless  
44 steel costs approximately four times higher than conventional carbon steel, it is suggested in  
45 studies that stainless steel structures are more economical on the basis of whole life than carbon  
46 steel in aggressive conditions [2].

47 Cold-formed sections are more common among stainless steel sections compared to hot-rolled  
48 and built-up sections in light structural applications [3]. There are various types of cold-formed  
49 sections including open sections and hollow sections. The cross-sections of doubly symmetric  
50 rectangular hollow flange beams (RHFBs) and triangular hollow flange beams (THFBs) are  
51 shown in Fig. 1. These sections can be formed by connecting the cold-formed hollow flanges  
52 to the web elements using electric resistance welding. The doubly symmetric hollow flange  
53 sections are more stable to the torsional effects than the monosymmetric hollow flange channel  
54 sections, and closed flanges suppress the distortional buckling effects which are more likely to  
55 appear in open sections with free edges such as C-sections and Z-sections. Therefore, doubly  
56 symmetric hollow flange sections are comparable in stability to commercially available I-  
57 sections and are found to be structurally efficient than conventional cold-formed sections.



58

59 Fig. 1 Doubly symmetric hollow flange sections

60 A number of researches have investigated the structural behaviour of hollow flange sections in  
 61 the past. Keerthan and Mahendran [4], [5] conducted experimental studies and numerical  
 62 investigations on the shear behaviour of cold-formed steel rectangular hollow flange channel  
 63 beams known as LiteSteel beams. Keerthan et al. [6], [7] investigated the combined bending  
 64 and shear response of rectangular hollow flange channel sections using experimental and  
 65 numerical studies. Moreover, both bending tests and numerical investigations have been  
 66 conducted on the rivet-fastened rectangular hollow flange channel beams by Siahaan et al. [8],  
 67 [9] while Wanniarachchi and Mahendran [10] experimented screw-fastened RHFBs to find out  
 68 section moment capacities. Also, the structural behaviour of cold-formed channel sections has  
 69 been thoroughly investigated by many researchers. Both experimental and numerical  
 70 investigations on cold-formed steel channel sections have been conducted by Pham and  
 71 Hancock [11]–[13] to study the combined bending and shear behaviour. The shear response of  
 72 lipped channel sections has been studied by Keerthan and Mahendran [14] for cold-formed  
 73 steel and Dissanayake et al. [15] for cold-formed stainless steel. In addition, the structural  
 74 response of I-sections has been investigated by a number of studies over the years. Olsson [16]  
 75 and Real et al. [17] performed shear tests on stainless steel plate girders while the bending and  
 76 shear interaction behaviour of stainless steel plate girders has been investigated by Saliba and  
 77 Gardner [18]. Further, the numerical investigations on lateral-torsional buckling behaviour of  
 78 stainless steel I-sections have been carried out by Saadat and Ashraf [19]. However, research  
 79 into cold-formed stainless steel hollow flange sections are relatively scarce.

80 The attention has been also given to the elastic shear buckling response of cold-formed sections  
 81 by a number of researches [20]–[22]. Keerthan and Mahendran [22] conducted shear buckling  
 82 analyses of different cold-formed sections including open and hollow flange beams using



83 numerical modelling. They proposed a generalised equation to calculate the shear buckling  
84 coefficients of cold-formed sections. The proposed equation takes into account the level of  
85 fixity of the web-to-flange juncture. It was suggested from the findings that the level of fixity  
86 at the web-to-flange juncture of RHFBS and THFBs is closer to fixed support conditions by  
87 Keerthan and Mahendran [22].

88 The direct strength method (DSM) has been adopted in the current North American  
89 specifications, AISI S100 [23] and Australian and New Zealand standards, AS/NZS 4600 [24]  
90 for the design of cold-formed steel sections. The DSM considers the whole section buckling  
91 when determining the section resistance, therefore, takes into account the element interaction  
92 in the design calculations. However, the current European standards for cold-formed steel,  
93 EN19931-3 [25] and for stainless steel, EN1993-1-4 [26] do not take into account the beneficial  
94 element interaction that present at the web-to-flange juncture [27]. Therefore, it is expected to  
95 provide conservative resistance predictions from European standards for hollow flange  
96 sections.

97 In this paper, the shear response of cold-formed stainless steel hollow flange sections (RHFBS  
98 and THFBs) is discussed. The details of numerical modelling conducted to investigate the shear  
99 response of RHFBS and THFBs and the use of numerical results in the evaluation of codified  
100 design provisions are presented.

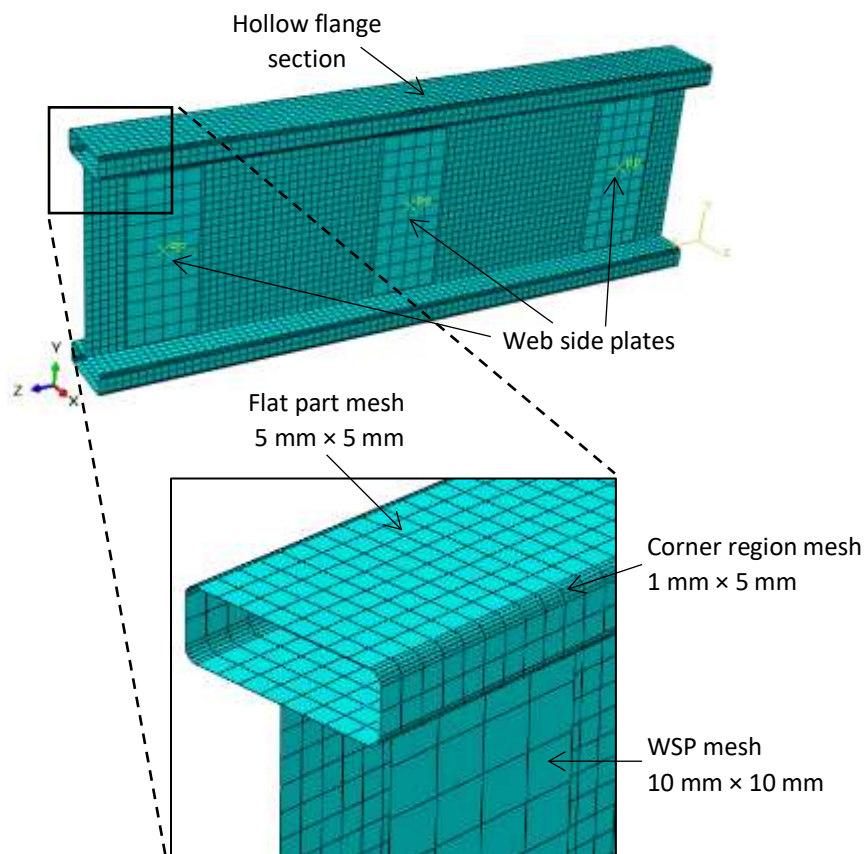
## 101 **2 Finite element (FE) modelling**

102 The numerical studies were conducted using commercially available FE software package  
103 ABAQUS CAE 2017 to investigate the shear response of cold-formed stainless steel hollow  
104 flange sections. The three-point loading setup used by Keerthan and Mahendran [4] in the shear  
105 tests of single LiteSteel beams were incorporated in the development of FE models. The details  
106 of numerical modelling and model validation are given in this section.

### 107 2.1 Development of FE model

108 In each FE model, single hollow flange sections were modelled together with three web side  
109 plates (WSPs) placed at the supports and at the loading point to simulate three-point loading  
110 tests. The quadrilateral four-node shell element with reduced integration, S4R was picked from  
111 the element library for the modelling of hollow flange sections. A 5 mm × 5 mm mesh was  
112 assigned for the flat parts of the sections while employing a relatively finer mesh of 1 mm × 5

113 mm to the corner regions following the mesh sensitivity analyses. The rigid quadrilateral  
114 element with four nodes, R3D4 was chosen to simulate the WSPs which have a relatively  
115 higher stiffness. The centre point of each plate was assigned as the rigid body reference point  
116 to which the motion of the rigid plates was then coupled. A 10 mm × 10 mm mesh was assigned  
117 to WSPs. Fig. 2 shows the different parts of the FE model and FE mesh.



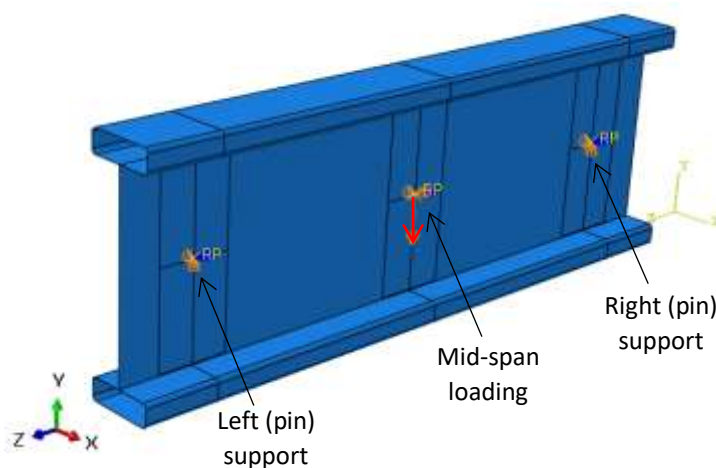
118

119 Fig. 2 Assembly of parts and FE mesh used in the modelling

120 In this study, recent proposals suggested by Arrayago et al. [28] to two-stage Ramberg-Osgood  
121 material model were incorporated to represent the non-linear material response of stainless  
122 steel while an elastic, perfectly-plastic material model was employed to model carbon steel  
123 behaviour in FE models. Then, stress-strain material data was fed into Abaqus in the form of  
124 true stress ( $\sigma_{true}$ ) and log plastic strain ( $\epsilon_{ln}^{pl}$ ). As a result of cold-work of forming, material  
125 properties of corner regions of stainless steel cross-sections are enhanced. A number of studies  
126 have investigated these strength enhancements and predictive models have been proposed  
127 [29]–[31]. These induced strengths in corner regions were explicitly considered in the  
128 numerical modelling and the more details of this can be found in [15]. The effects of residual

129 stresses were not incorporated in the numerical modelling of this study and were found to be  
130 negligible from similar numerical studies [5], [32], [33].

131 In the three-point loading tests, WSPs were attached to the section webs to eliminate any  
132 bearing failure that could occur at the supports or at the loading point. Therefore, in the FE  
133 models, boundary conditions and loading were assigned to the WSPs through the coupled rigid  
134 body reference points. Pin support conditions were employed at the two beam ends to maintain  
135 simply supported conditions. The in-plane translational DOFs of the cross-sectional plane (x-  
136 y plane) were restrained for the application of pin supports to the beam sections and the  
137 rotational DOF about the longitudinal axis (z-axis) of the section was restrained to avoid  
138 possible torsional effects. At the mid-span WSP, a downward displacement was applied to the  
139 reference point to simulate the loading of the section. The tie constraints available in Abaqus  
140 were employed to represent the bolted connections between section webs and WSPs. Fig. 3  
141 illustrates the assigned boundary conditions in the FE modelling.



142

143 Fig. 3 Assigned boundary conditions in the FE modelling

144 The effects of the local geometric imperfections on the performance of thin steel section  
145 behaviour is required to be taken into account in the numerical analysis. The details of  
146 numerical modelling of geometric imperfections have been reviewed in previous studies [34]–  
147 [36]. To calculate the magnitude of the local geometric imperfections ( $\omega_0$ ) of steel sections,  
148 Gardner and Nethercot [34] proposed modifications to the original prediction model developed  
149 by Dawson and Walker [37]. This modified Dawson and Walker model was employed in this  
150 study to represent the magnitude of the local geometric imperfections. This model is given by  
151 Eq. (1).

152  $\omega_0 = 0.023 \left( \frac{\sigma_{0.2}}{\sigma_{cr}} \right) t$  (1)

153 where  $\sigma_{0.2}$  is the 0.2 % proof stress of the material,  $\sigma_{cr}$  is the critical elastic buckling stress of  
 154 the most slender plate element of the section, and  $t$  is the cross-sectional thickness.

155 Two types of analysis were performed on each FE model. First, an Eigenvalue buckling  
 156 analysis was conducted to identify the critical buckling modes of the structure. These critical  
 157 modes were then introduced to the non-linear FE models to perturb the mesh to account for the  
 158 initial geometric imperfection patterns. Then, a geometrically and materially non-linear  
 159 analysis was performed on the FE models using a modified Static Riks analysis to investigate  
 160 the failure mechanism and the post-buckling behaviour of the sections.

161 2.2 Model validation

162 The shear tests conducted by Keerthan and Mahendran [4] on cold-formed steel hollow flange  
 163 channel sections (LiteSteel beams) were used for the validation. The compared hollow flange  
 164 sections have a shear span to clear web depth ratio (aspect ratio) of 1.0 to govern shear failure  
 165 in the sections. More details of the experiments can be found in [4].

166 The experimental and FE ultimate loads ( $V_{Exp.}$  and  $V_{FE}$ ) are compared in Table 1. From the  
 167 comparisons, it can be seen that experimental shear resistance to FE shear resistance ratio has  
 168 a mean of 0.99 and a coefficient of variation (COV) of 0.039. Therefore, it is clear that the  
 169 numerical models are able to predict the ultimate shear capacities of the hollow flange sections  
 170 accurately.

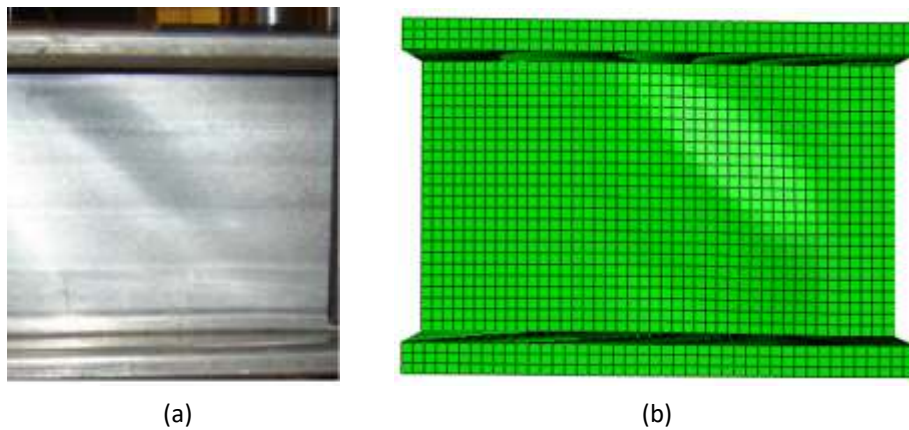
171 Table 1 Experimental [4] and FE shear resistances of LSBs

LSB section	$V_{Exp.}$ (kN)	$V_{FE}$ (kN)	$V_{Exp.}/V_{FE}$
LSB 150×45×15×2.0	68.5	69.84	0.98
LSB 200×60×20×2.0	88.2	87.54	1.01
LSB 200×60×20×2.5	119.3	115.64	1.03
LSB 250×75×25×2.5	139.6	137.88	1.01
LSB 300×75×25×2.5	143.7	155.28	0.93
Mean			0.99
COV			0.039

172

173 The cross-section designation: *Section name Section depth (D) × Section breadth (B) × Flange*  
174 *height (L) × Thickness (t)* was used to denote the considered cross-sections in this study. For  
175 an instance, a rectangular hollow flange channel section (LiteSteel beam) with a depth of 150  
176 mm, a breadth of 45 mm, a flange height of 15 mm and a thickness of 2.0 mm is denoted as  
177 *LSB 150×45×15×2.0*.

178 In addition, the failure mechanisms were compared to further assess the FE models with the  
179 experimental results. Fig. 4 illustrates the experimental and FE shear failure modes of *LSB*  
180 *150×45×15×2.0* section and the comparison is found to be fairly similar. Therefore, it can be  
181 concluded that the FE models simulate the shear failure mechanism of hollow flange sections  
182 reasonably well.



183

184 Fig. 4 (a) Experimental [4] and (b) FE shear failure mechanisms of *LSB 150×45×15×2.0* section

### 185 3 Numerical parametric study

#### 186 3.1 General

187 The influence of different cross-sectional dimensions and steel grades on the shear response of  
188 cold-formed stainless steel hollow flange sections were investigated utilising the validated  
189 numerical FE models. The shear response of RHFBS and THFBs were studied in this study.  
190 Two section heights (150 mm, 200 mm) and three section thicknesses (1 mm, 1.5 mm, 2 mm)  
191 were taken into account and four stainless steel grades including austenitic grades (1.4301,  
192 1.4311) and duplex grades (1.4362, 1.4462) were considered in the study. In addition, more  
193 slender 250 mm and 300 mm deep RHFBS, and 250 mm deep THFBs, of 1 mm thick and of  
194 stainless steel grade 1.4462 were developed to have a wide range of FE data. Altogether, 51  
195 FE models of stainless steel hollow flange beams were developed. The material properties for

196 stainless steel grades were found from EN1993-1-4 [26]. Young's modulus and Poisson's ratio  
197 were taken as 200,000 MPa and 0.3, respectively. Sections with an aspect ratio of 1.0 were  
198 used to govern the shear response.

### 199 3.2 FE shear resistances of hollow flange sections

200 The FE shear capacities of RHFBS and THFBs are summarised in Tables 2 and 3. Further, the  
201 comparisons of FE shear resistances with EN19931-4 [26] and the DSM predictions, and the  
202 proposed predictions are also included in tables. The details of these codified shear design  
203 provisions and the details of new proposals are discussed in Section 4.

204 Table 2 Parametric study results with EN1993-1-4 [26] and the DSM predictions for RHFB sections

Section	Stainless steel grade – 1.4301					Stainless steel grade – 1.4311					Stainless steel grade – 1.4362					Stainless steel grade – 1.4462				
	$V_{FE}$ (kN)	$V_{FE}/$ $V_{EC3}$	$V_{FE}/$ $V_{EC3,}$ Proposed	$V_{FE}/$ $V_{DSM}$	$V_{FE}/$ $V_{DSM,}$ Proposed	$V_{FE}$ (kN)	$V_{FE}/$ $V_{EC3}$	$V_{FE}/$ $V_{EC3,}$ Proposed	$V_{FE}/$ $V_{DSM}$	$V_{FE}/$ $V_{DSM,}$ Proposed	$V_{FE}$ (kN)	$V_{FE}/$ $V_{EC3}$	$V_{FE}/$ $V_{EC3,}$ Proposed	$V_{FE}/$ $V_{DSM}$	$V_{FE}/$ $V_{DSM,}$ Proposed	$V_{FE}$ (kN)	$V_{FE}/$ $V_{EC3}$	$V_{FE}/$ $V_{EC3,}$ Proposed	$V_{FE}/$ $V_{DSM}$	$V_{FE}/$ $V_{DSM,}$ Proposed
RHFB 150×45×15×1.0	18.84	1.50	1.09	1.35	1.16	21.57	1.45	1.03	1.33	1.11	29.72	1.47	1.00	1.37	1.09	32.27	1.48	1.01	1.39	1.09
RHFB 150×45×15×1.5	30.15	1.31	1.02	1.21	1.02	36.29	1.32	1.01	1.16	1.03	52.22	1.36	1.01	1.22	1.05	57.18	1.38	1.01	1.24	1.06
RHFB 150×45×15×2.0	45.31	1.18	1.02	1.37	1.01	54.12	1.24	1.02	1.30	1.01	77.32	1.32	1.02	1.19	1.02	84.49	1.32	1.02	1.17	1.03
RHFB 200×60×20×1.0	21.71	1.53	1.05	1.42	1.14	27.13	1.63	1.10	1.53	1.19	33.54	1.50	0.98	1.42	1.05	36.71	1.53	1.00	1.45	1.06
RHFB 200×60×20×1.5	34.18	1.28	0.95	1.14	0.99	41.82	1.32	0.96	1.19	1.02	60.18	1.38	0.96	1.28	1.04	65.75	1.40	0.97	1.30	1.05
RHFB 200×60×20×2.0	53.08	1.30	1.01	1.20	1.01	63.82	1.30	1.00	1.15	1.01	91.39	1.34	0.99	1.20	1.03	99.82	1.35	0.99	1.22	1.04
RHFB 250×75×25×1.0																40.84	1.60	1.02	1.52	1.05
RHFB 300×120×20×1.0																45.05	1.66	1.02	1.57	1.00

205

206

207

208

209

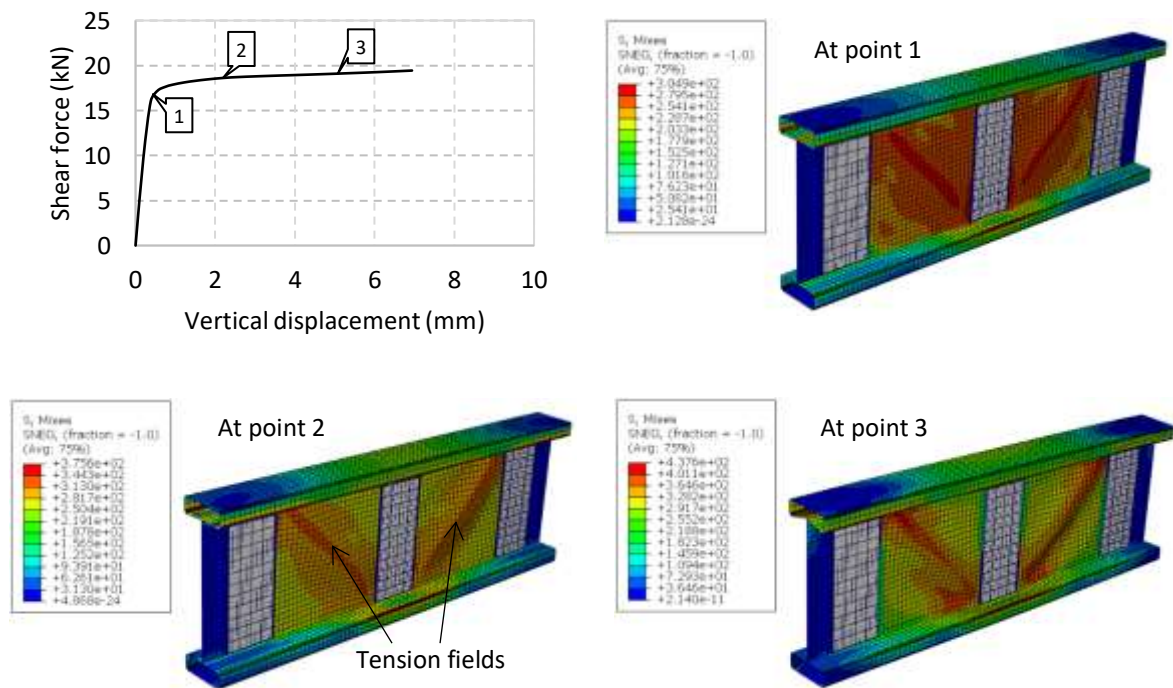
210 Table 3 Parametric study results with EN1993-1-4 [26] and the DSM predictions for THFB sections

Section	Stainless steel grade – 1.4301					Stainless steel grade – 1.4311					Stainless steel grade – 1.4362					Stainless steel grade – 1.4462				
	$V_{FE}$ (kN)	$V_{FE}/$ $V_{EC3}$	$V_{FE}/$ $V_{EC3}$ , Proposed	$V_{FE}/$ $V_{DSM}$	$V_{FE}/$ $V_{DSM}$ , Proposed	$V_{FE}$ (kN)	$V_{FE}/$ $V_{EC3}$	$V_{FE}/$ $V_{EC3}$ , Proposed	$V_{FE}/$ $V_{DSM}$	$V_{FE}/$ $V_{DSM}$ , Proposed	$V_{FE}$ (kN)	$V_{FE}/$ $V_{EC3}$	$V_{FE}/$ $V_{EC3}$ , Proposed	$V_{FE}/$ $V_{DSM}$	$V_{FE}/$ $V_{DSM}$ , Proposed	$V_{FE}$ (kN)	$V_{FE}/$ $V_{EC3}$	$V_{FE}/$ $V_{EC3}$ , Proposed	$V_{FE}/$ $V_{DSM}$	$V_{FE}/$ $V_{DSM}$ , Proposed
THFB 150×45×15×1.0	20.32	1.61	1.00	1.39	1.00	24.98	1.68	1.01	1.47	1.01	36.74	1.81	1.02	1.61	1.02	39.95	1.83	1.01	1.64	1.01
THFB 150×45×15×1.5	34.30	1.49	1.00	1.38	1.00	41.44	1.50	0.99	1.32	0.99	59.85	1.56	0.99	1.34	0.98	65.74	1.59	0.99	1.37	0.99
THFB 150×45×15×2.0	50.11	1.31	1.03	1.51	1.01	59.77	1.37	0.99	1.43	0.99	85.21	1.45	0.97	1.31	0.97	93.54	1.47	0.97	1.30	0.97
THFB 200×60×20×1.0	25.02	1.76	1.01	1.56	1.01	30.99	1.86	1.02	1.66	1.02	45.19	2.02	1.02	1.82	1.02	49.19	2.05	1.02	1.85	1.02
THFB 200×60×20×1.5	42.15	1.57	1.00	1.34	1.00	51.56	1.62	1.01	1.40	1.01	74.88	1.72	1.01	1.52	1.00	82.10	1.75	1.01	1.55	1.01
THFB 200×60×20×2.0	61.11	1.49	1.01	1.38	1.00	73.68	1.50	0.99	1.32	0.99	106.36	1.56	0.99	1.34	0.98	117.09	1.59	0.99	1.37	0.99
THFB 250×75×25×1.0																56.66	2.22	1.00	2.01	1.00



212 3.3 Results discussion

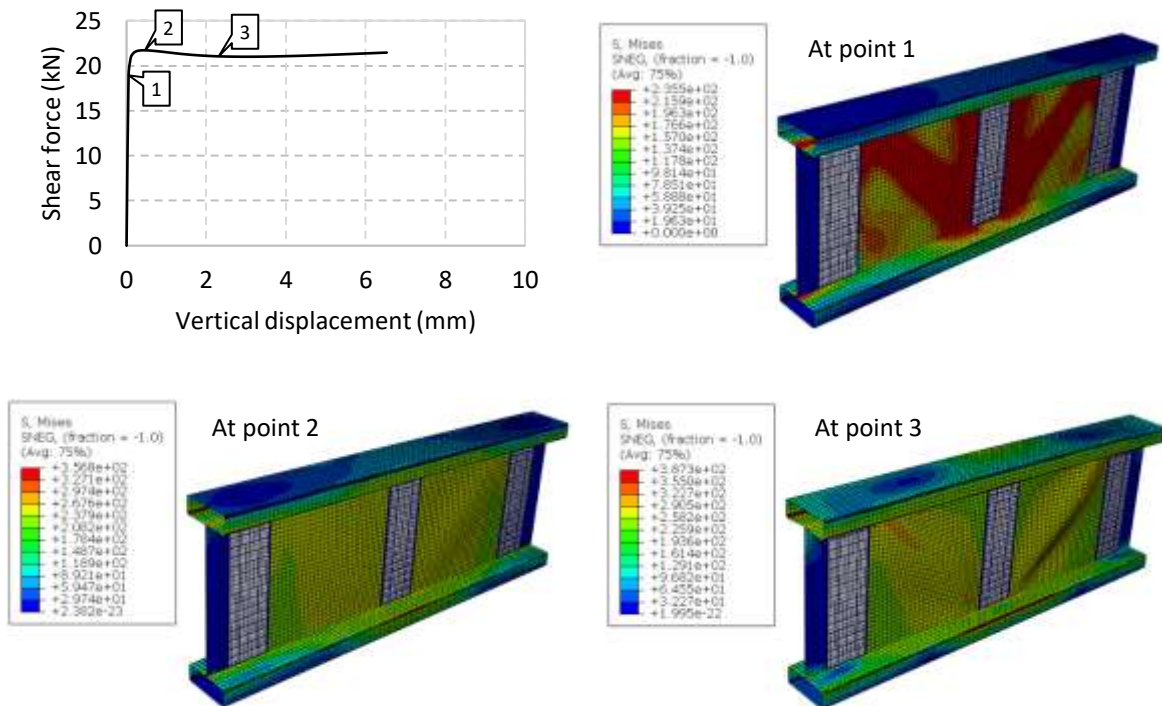
213 The shear response of cold-formed stainless steel RHFB sections and THFB sections are  
 214 discussed in this section using the generated numerical FE results in the parametric study. Fig.  
 215 5 illustrates the shear response of *RHFB 150×45×15×1.0* section of stainless steel grade  
 216 1.4301 with its load-deflection curve while Fig. 6 shows that of *RHFB 200×60×20×1.0* section  
 217 of the same steel grade. From Figs. 5 and 6, it can be seen that the out-of-plane buckling of  
 218 section webs approximately start at point 1 where a change in section stiffness can be observed  
 219 from the load-deflection curves. Then, the progressive buckling of both section webs at the  
 220 failure point and at the post-failure regime can be observed under the shear loading. Further,  
 221 the formed diagonal tension bands of highly stressed regions are clearly visible in *RHFB*  
 222 *150×45×15×1.0* section as a result of the anchoring provided to the webs by the transverse  
 223 web stiffeners and flanges. However, these tension fields are normalised over the section webs  
 224 in *RHFB 200×60×20×1.0* section.



225

226 Fig. 5 Shear response of *RHFB 150×45×15×1.0* section at the different stages of load-deflection curve

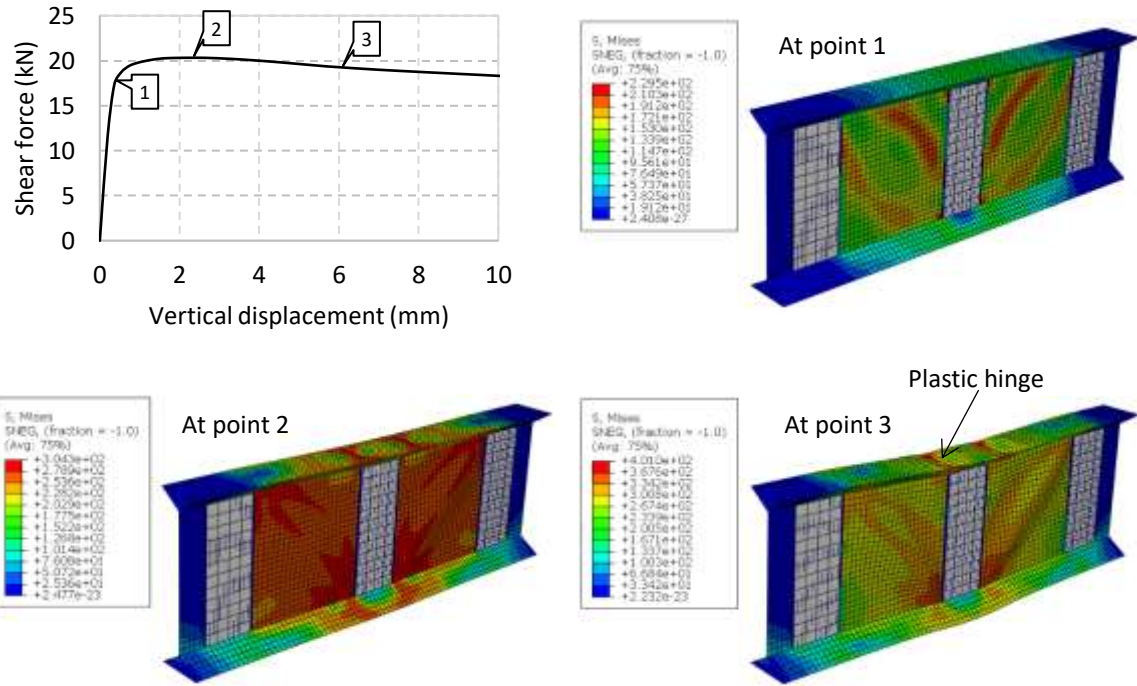
227



228

229 Fig. 6 Shear response of *RHFB 200×60×20×1.0* section at the different stages of load-deflection curve

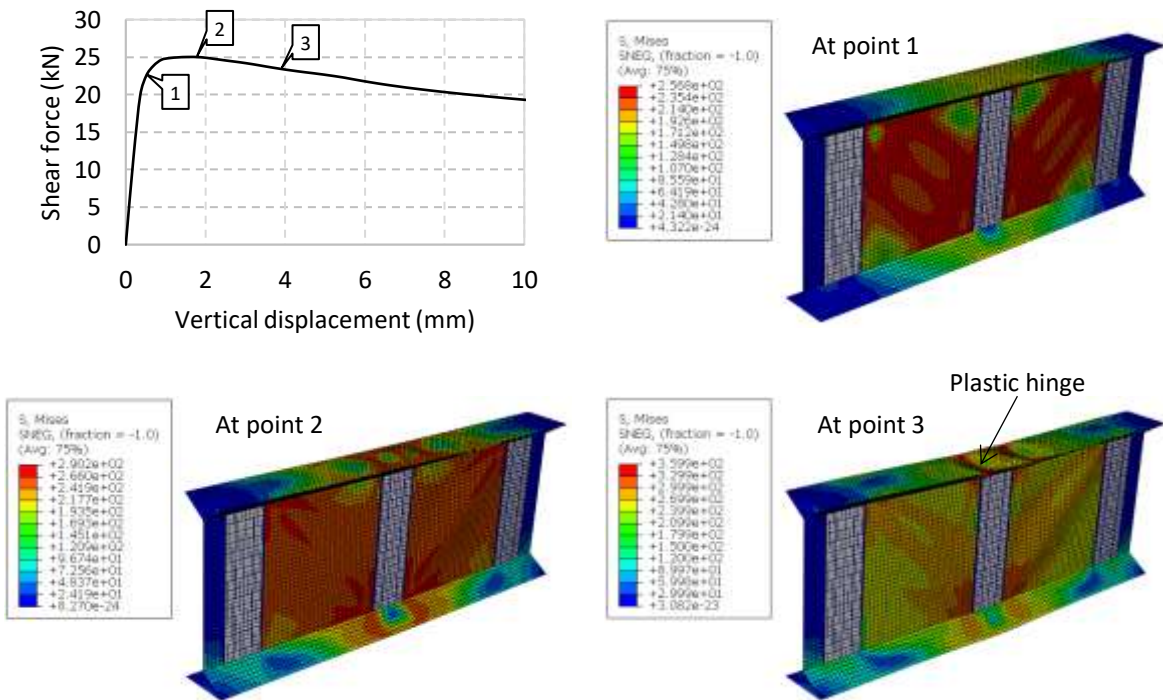
230 Figs. 7 and 8 illustrate the shear behaviour of *THFB 150×45×15×1.0* section and *THFB*  
 231 *200×60×20×1.0* section of stainless steel grade 1.4301, respectively with their load-deflection  
 232 curves. Both sections begin to show signs of out-of-plane buckling of webs at around point 1  
 233 of their load-deflection curves. After this, the progression of web shear buckling of both  
 234 sections can be observed through their failure points. The increased anchoring facilitated by  
 235 the triangular flanges and transverse web stiffeners caused the distribution of the stresses in the  
 236 webs more evenly. Therefore, the diagonal tension bands are not clearly visible in THFB  
 237 sections as opposed to RHFB sections. Moreover, a plastic hinge type mechanism is formed in  
 238 the mid-span of THFB sections at the post-failure region. The excessive compression stresses  
 239 induced within the triangular top flanges as a result of the anchoring provided by the top flanges  
 240 to the tension fields could lead to this formation.



241

242 Fig. 7 Shear response of THFB 150×45×15×1.0 section at the different stages of load-deflection curve

243



244

245 Fig. 8 Shear response of THFB 200×60×20×1.0 section at the different stages of load-deflection curve

#### 246 4 Assessment of shear design rules

247 The generated numerical database of hollow flange sections was incorporated in this section to  
248 evaluate the shear design rules provided in European standards for stainless steel [26] and the  
249 DSM shear design rules. Following the assessment of codified shear provisions, new shear  
250 design equations were proposed using FE results.

##### 251 4.1 European standards for stainless steel, EN1993-1-4 [26]

252 European standards for stainless steel [26] adopts the shear design rules provided in European  
253 standards for plated steel, EN1993-1-5 [38]. According to that, the summation of the shear  
254 buckling resistance of the section web ( $V_{bw,Rd}$ ) and the flange contribution to the shear  
255 resistance of the section ( $V_{bf,Rd}$ ) gives the shear resistance of the section ( $V_{b,Rd}$ ) as expressed in  
256 Eq. (2).

$$257 \quad V_{b,Rd} = V_{bw,Rd} + V_{bf,Rd} \leq \frac{\eta f_{yw} h_w t_w}{\sqrt{3} \gamma_{M1}} \quad (2)$$

258 where the parameter  $\eta$  takes into account the strain hardening of stainless steel,  $\gamma_{M1}$  is the partial  
259 safety factor,  $f_{yw}$  is the yield strength of the web,  $h_w$  is the depth of the web, and  $t_w$  is the  
260 thickness of the web.

261 The shear buckling resistance of the web ( $V_{bw,Rd}$ ) is given by Eq. (3) in which  $\chi_w$  is the web  
262 shear buckling reduction factor.

$$263 \quad V_{bw,Rd} = \frac{\chi_w f_{yw} h_w t_w}{\sqrt{3} \gamma_{M1}} \quad (3)$$

264 The flange contribution ( $V_{bf,Rd}$ ) is defined by Eq. (4).

$$265 \quad V_{bf,Rd} = \frac{b_f t_f^2 f_{yf}}{c \gamma_{M1}} \left( 1 - \left( \frac{M_{Ed}}{M_{f,Rd}} \right)^2 \right) \quad (4)$$

266 where  $b_f$  is the width of the flange,  $t_f$  is the thickness of the flange, and  $f_{yf}$  is the yield strength  
267 of the flange.  $M_{Ed}$  is the design bending moment of the section and  $M_{f,Rd}$  is the moment  
268 resistance of the flanges alone. The parameter  $c$  is the distance to the location of the plastic  
269 hinge from the transverse stiffener. Eq. (5) is given in EN1993-1-4 [26] to calculate the  
270 parameter  $c$ .

$$271 \quad c = a \left[ 0.17 + \frac{3.5 b_f t_f^2 f_{yf}}{t_w h_w^2 f_{yw}} \right] \text{ and } \frac{c}{a} \leq 0.65 \quad (5)$$

272 where  $a$  is the length of the shear panel.

273 Two sets of expressions are set out in EN1993-1-4 [26] to calculate the web shear buckling  
274 reduction factor ( $\chi_w$ ) of the section webs with and without rigid end posts. These expressions  
275 for the webs with rigid end posts are given by Eqs. (6)-(8).

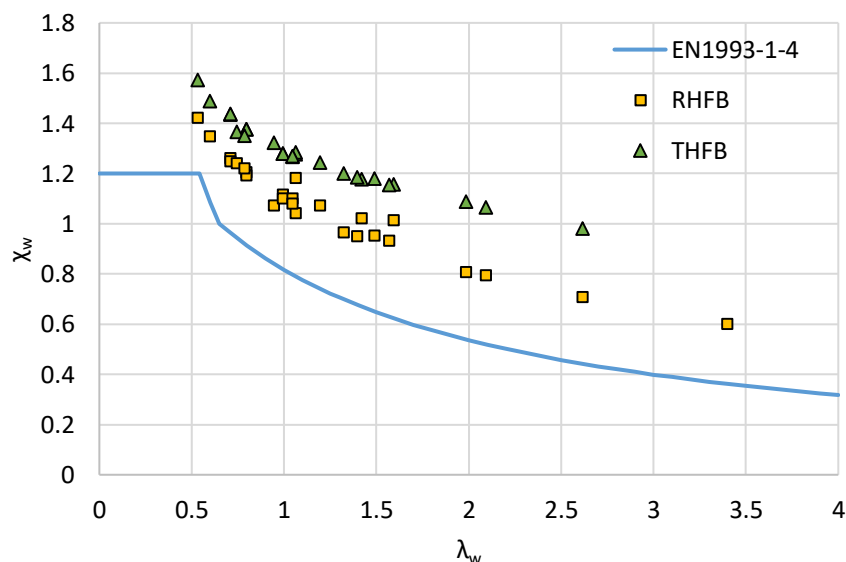
276 
$$\chi_w = \eta \text{ for } \bar{\lambda}_w \leq 0.65/\eta \tag{6}$$

277 
$$\chi_w = 0.65/\bar{\lambda}_w \text{ for } 0.65/\eta < \bar{\lambda}_w < 0.65 \tag{7}$$

278 
$$\chi_w = 1.56/(0.91 + \bar{\lambda}_w) \text{ for } \bar{\lambda}_w \geq 0.65 \tag{8}$$

279 where  $\bar{\lambda}_w$  is the slenderness of the web.

280 The EN1993-1-4 [26] shear design rules were then evaluated using the numerical FE results  
281 generated in Section 3 to assess their applicability to predict the shear resistance of cold-formed  
282 stainless steel hollow flange sections. The comparison of EN1993-1-4 [26] shear design rules  
283 with FE results for each section is given in Tables 2 and 3. The generated numerical shear  
284 capacities are plotted with EN1993-1-4 [26] web shear buckling reduction factor ( $\chi_w$ ) in Fig. 9  
285 and can be seen that the codified shear provisions are too conservative for cold-formed stainless  
286 steel hollow flange sections. Further, THFBs are found to have higher shear resistances than  
287 RHFBs.



288

289 Fig. 9 Comparison of FE shear capacities with the web shear buckling reduction factor ( $\chi_w$ ) of EN1993-1-4 [26]

290 Table 4 summarises the overall mean and COV of FE shear resistance to predicted shear  
291 resistance ratio for each cross-section type. The conservative nature of EN1993-1-4 [26] shear

292 capacity predictions for hollow flange sections is further confirmed from mean and COV  
 293 values. Eurocode provisions do not take into account the favourable effect of fixity at the web-  
 294 to-flange juncture of the hollow flange sections to shear buckling resistance of the section web  
 295 could be one reason for these conservative predictions.

296 Table 4 Overall mean and COV of FE to predicted shear resistance ratio for each section type

	EN1993-1-4 [26]		DSM	
	Current	Proposed	Current	Proposed
RHFBs				
Mean	1.40	1.01	1.30	1.05
COV	0.087	0.034	0.097	0.048
THFBs				
Mean	1.66	1.00	1.49	1.00
COV	0.132	0.015	0.127	0.015

297

298 Therefore, Eurocode shear provisions were modified to enhance the shear resistance prediction  
 299 accuracy of stainless steel hollow flange sections. The new set of expressions for web shear  
 300 buckling reduction factor ( $\chi_w$ ) of EN1993-1-4 [26] were proposed using numerical FE shear  
 301 capacities of hollow flange sections and following regression analyses. The elastic shear  
 302 buckling coefficients proposed for RHFBs and THFBs by Keerthan and Mahendran [22] were  
 303 utilised here when modifying the codified expressions. Therefore, proposed shear provisions  
 304 do take into account the available fixity at the web-to-flange juncture.

305 The proposed expressions for web shear buckling reduction factor ( $\chi_w$ ) of RHFBs are given by  
 306 Eqs. (9)-(11).

$$307 \chi_w = 1.4 \text{ for } \bar{\lambda}_w \leq 0.5 \quad (9)$$

$$308 \chi_w = 1.08/\bar{\lambda}_w^{0.34} \text{ for } 0.5 < \bar{\lambda}_w < 1.25 \quad (10)$$

$$309 \chi_w = 2.75/(1.5 + \bar{\lambda}_w) \text{ for } \bar{\lambda}_w \geq 1.25 \quad (11)$$

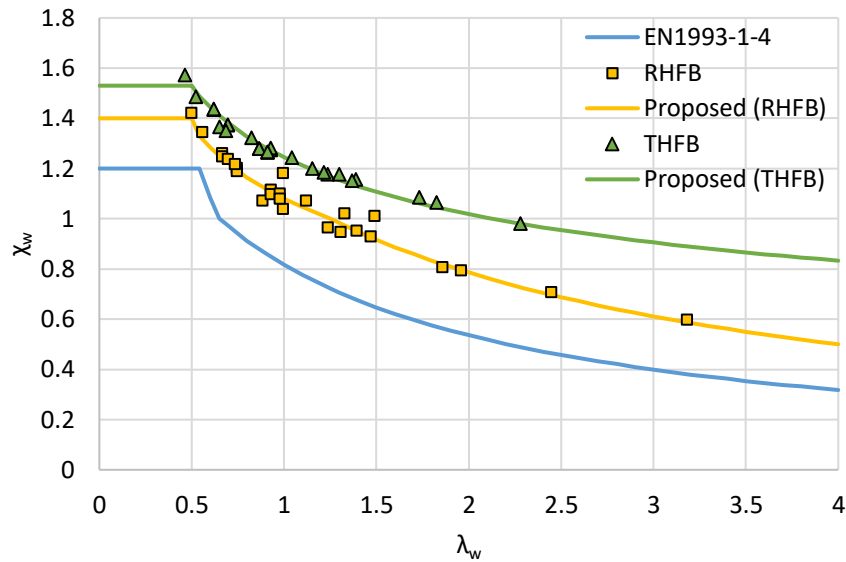
310 Eqs. (12) and (13) provides the modified expressions for web shear buckling reduction factor  
 311 ( $\chi_w$ ) of THFBs.

$$312 \chi_w = 1.53 \text{ for } \bar{\lambda}_w \leq 0.5 \quad (12)$$

$$313 \chi_w = 1.245/\bar{\lambda}_w^{0.29} \text{ for } 0.5 < \bar{\lambda}_w \quad (13)$$

314 Fig. 10 plots the proposed expressions for web shear buckling reduction factor ( $\chi_w$ ) for stainless  
 315 steel hollow flange sections with FE shear capacities. It can be seen that the proposed curves

316 are fitted well with the distribution of the corresponding FE results, therefore, suggesting better  
 317 prediction accuracy over the codified web shear buckling curve of EN1993-1-4 [26]. The mean  
 318 and COV of proposed EN1993-1-4 [26] provisions given in Table 4 also implies the improved  
 319 shear resistance predictions for both section types over the current shear provisions.



320  
 321 Fig. 10 Comparison of FE shear capacities with the proposed web shear buckling reduction factor ( $\chi_w$ ) for  
 322 EN1993-1-4 [26]

### 323 4.2 The direct strength method

324 The DSM has been developed as an alternative design approach to the traditional cross-section  
 325 classification framework known as the effective width method. The clause 7.2.3.3 of Australian  
 326 and New Zealand standards, AS/NZS 4600 [24] includes the details of the DSM shear design  
 327 rules for the sections with transverse web stiffeners.

328 The sectional shear capacity ( $V_v$ ) according to the DSM is given by Eqs. (14) and (15).

$$329 V_v = V_y \text{ for } \lambda \leq 0.776 \quad (14)$$

$$330 V_v = \left[ 1 - 0.15 \left( \frac{1}{\lambda^2} \right)^{0.4} \right] \left( \frac{1}{\lambda^2} \right)^{0.4} V_y \text{ for } \lambda > 0.776 \quad (15)$$

331 where  $\lambda$  is the cross-sectional slenderness.

332 The slenderness of the cross-section,  $\lambda$  is defined as in Eq. (16) using the shear yield capacity  
 333 of the section ( $V_y$ ) and the elastic shear buckling capacity of the section ( $V_{cr}$ ).

334 
$$\lambda = \sqrt{\frac{V_y}{V_{cr}}} \tag{16}$$

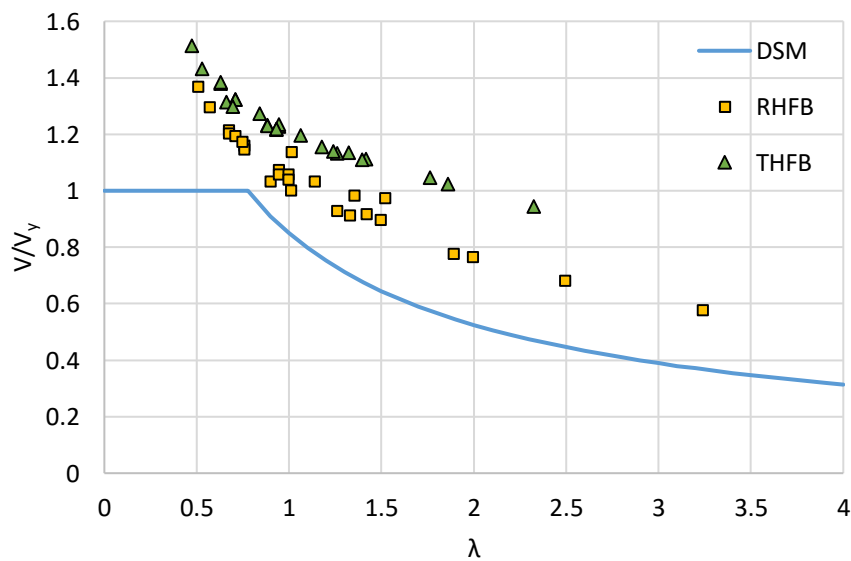
335 Eqs. (17) and (18) can be used to calculate the shear yield capacity ( $V_y$ ) and the elastic shear  
 336 buckling capacity ( $V_{cr}$ ) of the section.

337 
$$V_y = 0.6 f_{yw} d_1 t_w \tag{17}$$

338 
$$V_{cr} = \frac{k\pi^2 E}{12(1-\nu^2)} \frac{t_w^3}{d_1} \tag{18}$$

339 where  $f_{yw}$  is the yield strength of the web,  $d_1$  is the flat depth of the web,  $t_w$  is the thickness of  
 340 the web,  $E$  is Young's modulus,  $\nu$  is Poisson's ratio, and  $k$  is the elastic shear buckling  
 341 coefficient of the section.

342 The applicability of the DSM shear design provisions to predict the section capacities of cold-  
 343 formed stainless steel hollow flange sections were then assessed using the numerical parametric  
 344 study results gathered in Section 3. The elastic shear buckling coefficient ( $k$ ) of the hollow  
 345 flange sections were found from Keerthan and Mahendran [22]. Fig. 11 illustrates the FE shear  
 346 capacities of RHFBs and THFBs together with the DSM shear design curve. Moreover, the  
 347 overall mean and COV of FE shear capacity to DSM predicted shear capacity ratio for each  
 348 hollow flange section type is given in Table 4. Both these comparisons reflect that the DSM  
 349 shear design provisions significantly under-predict the section capacities of stainless steel  
 350 RHFBs and THFBs as similar to EN1993-1-4 [26] shear design provisions.



351

352 Fig. 11 Comparison of FE shear capacities with the DSM shear design curve



353 Following the assessment of DSM shear design rules, modifications were made to Eqs. (16)  
354 and (17) aiming to achieve improved shear capacity predictions for the cold-formed stainless  
355 steel hollow flange sections. Regression analyses were conducted to fit the proposed DSM  
356 curves to FE shear capacities.

357 The proposed DSM equations for stainless steel RHFB sections are expressed in Eqs. (19)-  
358 (21).

$$359 \quad V_v = 1.36V_y \text{ for } \lambda \leq 0.5 \quad (19)$$

$$360 \quad V_v = \frac{V_y}{\lambda^{0.444}} \text{ for } 0.5 < \lambda \leq 1.0 \quad (20)$$

$$361 \quad V_v = \left[ 1 - 0.01 \left( \frac{1}{\lambda^2} \right)^{0.232} \right] \left( \frac{1}{\lambda^2} \right)^{0.232} V_y \text{ for } \lambda > 1.0 \quad (21)$$

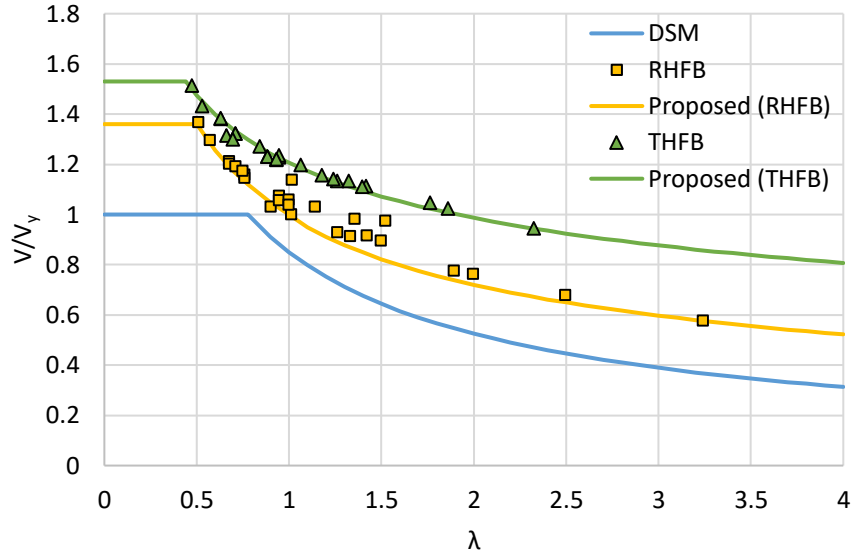
362 Eqs. (22) and (23) provide the proposed DSM equations for stainless steel THFB sections.

$$363 \quad V_v = 1.53V_y \text{ for } \lambda \leq 0.44 \quad (22)$$

$$364 \quad V_v = \frac{1.206V_y}{\lambda^{0.29}} \text{ for } \lambda > 0.44 \quad (23)$$

365 The new DSM equations and existing DSM equations for shear are plotted together with the  
366 FE capacities of stainless steel RHFBs and THFBs in Fig. 12. The comparison shows that the  
367 proposed DSM curves follow the distribution of the respective FE results well. Further, the  
368 mean and COV of proposed DSM provisions given in Table 4 suggest enhanced capacity  
369 predictions for stainless steel hollow flange sections over the current DSM shear design rules.

370



371

372 Fig. 12 Comparison of FE shear capacities with the proposed DSM shear design curve

### 373 4.3 Reliability analysis

374 Reliability analysis was conducted for the proposed EN1993-1-4 [26] and the DSM resistance  
 375 models according to North American specifications for cold-formed steel [23]. The capacity  
 376 reduction factor ( $\phi_v$ ) of each resistance model was calculated using Eq. (24).

$$377 \quad \phi_v = 1.52M_m F_m P_m e^{-\beta_0 \sqrt{(V_m^2 + V_f^2 + C_p V_p^2 + V_q^2)}} \quad (24)$$

378 where  $M_m=1.1$  and  $V_m=0.1$  are mean and COV of the material factor, respectively.  $F_m=1.0$  and  
 379  $V_f=0.05$  are mean and COV of the fabrication factor, respectively.  $P_m$  and  $V_p$  (not less than  
 380 0.065) are mean and COV of the actual (FE) resistance to predicted resistance ratio,  
 381 respectively.  $\beta_0$  is the target reliability index and  $V_q=0.21$  is the COV of the load effect.

382 The correction factor,  $C_p$  is given by Eq. (25).

$$383 \quad C_p = \left[ 1 + \frac{1}{n} \right] \left[ \frac{m}{m-2} \right] \quad (25)$$

384 where  $m=n-1$  and  $n$  is the total number of data.

385 For the calculations, the target reliability index,  $\beta_0$  was taken as 2.5 and the minimum  
 386 recommended value was assigned for  $V_p$  as the actual values were found to be less than 0.065.  
 387 The calculated capacity reduction factors for the proposed EN1993-1-4 [26] resistance models  
 388 are 0.91 for RHFb's and 0.90 for THFB's. For the proposed DSM resistance models, the  
 389 calculated capacity reduction factors are found to be 0.95 for RHFb's and 0.90 for THFB's.

390 Therefore, a value of 0.90 is recommended in general for the capacity reduction factor of all  
391 the resistance functions.

## 392 **5 Concluding remarks**

393 The shear response of cold-formed stainless steel hollow flange sections was investigated using  
394 numerical analysis in this paper. The numerical parametric studies were conducted for RHFB  
395 sections and THFB sections using the validated FE models. Various influential parameters such  
396 as the height of the section, the thickness of the section and the steel grade were taken into  
397 account in the study and 51 FE models of hollow flange sections were developed. The  
398 numerical results were used to observe the shear response of the sections and to evaluate the  
399 codified shear provisions. From the FE results, it can be observed that diagonal tension fields  
400 are formed within section webs of RHFB sections however more even distribution of the  
401 stresses can be seen in the webs of THFB sections with no clearly visible tension bands as a  
402 result of increased anchoring provided by the flanges. The increased anchoring provided by the  
403 flanges results into developing plastic hinge type mechanism in the top flanges of THFB  
404 sections at the mid-span. Moreover, the shear resistance of THFBs is found to be relatively  
405 higher than RHFBs. In general, the evaluation of EN1993-1-4 [26] and the DSM shear design  
406 rules using the generated numerical results suggests that the current codified provisions  
407 considerably under-predict the shear resistance of stainless steel hollow flange sections.  
408 Therefore, modifications were proposed to the codified provisions aiming improved shear  
409 capacity predictions. The proposed shear provisions offer more accurate and consistent shear  
410 capacity predictions over the codified provisions. The reliability of the proposed provisions  
411 was also assessed.

## 412 **Acknowledgements**

413 Authors would like to thank Northumbria University for financial support and providing the  
414 necessary research facilities to conduct this research.

## 415 **References**

- 416 [1] N. R. Baddoo, Stainless steel in construction: A review of research, applications,  
417 challenges and opportunities, *J. Constr. Steel Res.* 64 (11) (2008) pp. 1199–1206.
- 418 [2] L. Gardner, Aesthetics, economics and design of stainless steel structures, *Adv. Steel*  
419 *Constr.* 4 (2) (2008) pp. 113–122.

- 420 [3] L. Gardner, The use of stainless steel in structures, *Pro. Struct. Eng. Mater.* 7 (2) (2005)  
421 pp. 45–55.
- 422 [4] P. Keerthan, M. Mahendran, Experimental studies on the shear behaviour and strength  
423 of LiteSteel beams, *Eng. Struct.* 32 (10) (2010) pp. 3235–3247.
- 424 [5] P. Keerthan, M. Mahendran, New design rules for the shear strength of LiteSteel beams,  
425 *J. Constr. Steel Res.* 67 (6) (2011) pp. 1050–1063.
- 426 [6] P. Keerthan, D. Hughes, M. Mahendran, Experimental studies of hollow flange channel  
427 beams subject to combined bending and shear actions, *Thin-Walled Struct.* 77 (2014)  
428 pp. 129–140.
- 429 [7] P. Keerthan, M. Mahendran, D. Hughes, Numerical studies and design of hollow flange  
430 channel beams subject to combined bending and shear actions, *Eng. Struct.* 75 (2014)  
431 pp. 197–212.
- 432 [8] R. Siahayan, M. Mahendran, P. Keerthan, Section moment capacity tests of rivet  
433 fastened rectangular hollow flange channel beams, *J. Constr. Steel Res.* 125 (2016) pp.  
434 252–262.
- 435 [9] R. Siahayan, P. Keerthan, M. Mahendran, Finite element modeling of rivet fastened  
436 rectangular hollow flange channel beams subject to local buckling, *Eng. Struct.* 126  
437 (2016) pp. 311–327.
- 438 [10] K. S. Wanniarachchi, M. Mahendran, Experimental study of the section moment  
439 capacity of cold-formed and screw-fastened rectangular hollow flange beams, *Thin-  
440 Walled Struct.* 119 (2017) pp. 499–509.
- 441 [11] C. H. Pham, G. J. Hancock, Experimental investigation of high strength cold-formed  
442 C-sections in combined bending and shear, *J. Struct. Eng.* 136 (7) (2010) pp. 866–878.
- 443 [12] C. H. Pham, G. J. Hancock, Numerical simulation of high strength cold-formed purlins  
444 in combined bending and shear, *J. Constr. Steel Res.* 66 (10) (2010) pp. 1205–1217.
- 445 [13] C. H. Pham, G. J. Hancock, Direct strength design of cold-formed C-sections for shear  
446 and combined actions, *J. Struct. Eng.* 138 (6) (2012) pp. 759–768.
- 447 [14] P. Keerthan, M. Mahendran, Experimental investigation and design of lipped channel  
448 beams in shear, *Thin-Walled Struct.* 86 (2015) pp. 174–184.
- 449 [15] D. M. M. P. Dissanayake, K. Poologanathan, S. Gunalan, K. D. Tsavdaridis, B.  
450 Nagaratnam, K. S. Wanniarachchi, Numerical modelling and shear design rules of  
451 stainless steel lipped channel sections, *J. Constr. Steel Res.* (2019) (In press).
- 452 [16] A. Olsson, Stainless steel plasticity-material modelling and structural applications, PhD  
453 thesis, Lulea University of Technology, Sweden, 2001.

- 454 [17] E. Real, E. Mirambell, I. Estrada, Shear response of stainless steel plate girders, *Eng.*  
455 *Struct.* 29 (7) (2007) pp. 1626–1640.
- 456 [18] N. Saliba, L. Gardner, Experimental study of the shear response of lean duplex stainless  
457 steel plate girders, *Eng. Struct.* 46 (2013) pp. 375–391.
- 458 [19] M. Anwar-Us-Saadat, M. Ashraf, The continuous strength method for lateral-torsional  
459 buckling of stainless steel I-beams, *Thin-Walled Struct.* 130 (2018) pp. 148–160.
- 460 [20] C. H. Pham, G. J. Hancock, Shear buckling of thin-walled channel sections, *J. Constr.*  
461 *Steel Res.* 65 (3) (2009) pp. 578–585.
- 462 [21] C. H. Pham, G. J. Hancock, Elastic buckling of cold-formed channel sections in shear,  
463 *Thin-Walled Struct.* 61 (2012) pp. 22–26.
- 464 [22] P. Keerthan, M. Mahendran, Improved shear design rules of cold-formed steel beams,  
465 *Eng. Struct.* 99 (2015) pp. 603–615.
- 466 [23] AISI S100–16, North American Specification for the design of cold-formed steel  
467 structural members, American Iron and Steel Institute (AISI), Washington, 2016.
- 468 [24] AS/NZS 4600, Cold-formed steel structures, Standards Australia/Standards New  
469 Zealand (AS/NZS), Sydney, 2018.
- 470 [25] EN 1993-1-3, Eurocode 3 – Design of steel structures – Part 1–3: General rules –  
471 Supplementary rules for cold-formed members and sheeting, European Committee for  
472 Standardization (CEN), Brussels, 2006.
- 473 [26] EN 1993-1-4:2006+A1:2015, Eurocode 3 – Design of steel structures – Part 1–4:  
474 General rules – Supplementary rules for stainless steels, European Committee for  
475 Standardization (CEN), Brussels, 2015.
- 476 [27] O. Zhao, S. Afshan, L. Gardner, Structural response and continuous strength method  
477 design of slender stainless steel cross-sections, *Eng. Struct.* 140 (2017) pp. 14–25.
- 478 [28] I. Arrayago, E. Real, L. Gardner, Description of stress-strain curves for stainless steel  
479 alloys, *Mater. Des.* 87 (2015) pp. 540–552.
- 480 [29] M. Ashraf, L. Gardner, D. A. Nethercot, Strength enhancement of the corner regions of  
481 stainless steel cross-sections, *J. Constr. Steel Res.* 61 (1) (2005) pp. 37–52.
- 482 [30] R. B. Cruise, L. Gardner, Strength enhancements induced during cold forming of  
483 stainless steel sections, *J. Constr. Steel Res.* 64 (11) (2008) pp. 1310–1316.
- 484 [31] B. Rossi, S. Afshan, L. Gardner, Strength enhancements in cold-formed structural  
485 sections – Part II: Predictive models, *J. Constr. Steel Res.* 83 (2013) pp. 189–196.

- 486 [32] S. Niu, K. J. R. Rasmussen, F. Fan, Distortional-global interaction buckling of stainless  
487 steel C-beams: Part II - Numerical study and design, *J. Constr. Steel Res.* 96 (2014) pp.  
488 40–53.
- 489 [33] Y. Liang, O. Zhao, Y. Long, L. Gardner, Stainless steel channel sections under  
490 combined compression and minor axis bending – part 1: experimental study and  
491 numerical modelling, *J. Constr. Steel Res.* 152 (2019) pp. 154–161.
- 492 [34] L. Gardner, D. A. Nethercot, Numerical modeling of stainless steel structural  
493 components–A consistent approach, *J. Struct. Eng.* 130 (10) (2004) pp. 1586–1601.
- 494 [35] M. Ashraf, L. Gardner, D. A. Nethercot, Geometric imperfections in stainless steel  
495 cross-sections, *Proceedings of the Fourth International Conference on Advances in*  
496 *Steel Structures*, 13–15 June 2005, Shanghai, China, pp. 105–112.
- 497 [36] M. Ashraf, L. Gardner, D. A. Nethercot, Finite element modelling of structural stainless  
498 steel cross-sections, *Thin-Walled Struct.* 44 (10) (2006) pp. 1048–1062.
- 499 [37] R. G. Dawson, A. C. Walker, Post-buckling of geometrically imperfect plates, *J. Struct.*  
500 *Div.* 98 (1) (1972) pp. 75–94.
- 501 [38] EN 1993-1-5, Eurocode 3 – Design of steel structures – Part 1–5: Plated structural  
502 elements, European Committee for Standardization (CEN), Brussels, 2006.